Journal of Applied Fluid Mechanics, Vol. 13, No. 3, pp. 969-979, 2020.
Available online at www.jafmonline.net, ISSN 1735-3572, EISSN 1735-3645.
DOI: 10.29252/jafm.13.03.30688

Numerical Study on a Novel Type of High Gravity Rotary Gas-Liquid Separator

Z. Zhang, H. Wang, J. Ma† and X. Ling

School of Mechanical and Power Engineering, Nanjing Tech University, Nanjing, Jiangsu, 211816, China

†*Corresponding Author Email: jiema@njtech.edu.cn*

(Received June 28, 2019; accepted November 4, 2019)

ABSTRACT

In textile printing and dyeing industry, a novel type of separator called high gravity rotary gas-liquid separator (HGRGS) is designed, which includes a rotary drum with multi-layer fins and an impeller. First, the structure and separation principle of HGRGS are introduced in this paper. Then, the flow field and separation efficiency are studied by CFD techniques. To ensure the accuracy of the numerical simulation, the results are verified by the available experimental data. Compared with the typical cyclone, the maximum pressure drop reduction rate in HGRGS is 64.7% when the gas enters at 10 m/s. Besides, for droplets less than 5 μm, the separation performance in HGRGS is more efficient and it will be greatly improved by 30% for 1 μm droplets. The numerical results also show that the tangential velocity inside the rotary drum is linear with the radius and the higher the rotating speed, the greater the tangential velocity. Moreover, the maximum tangential velocity between the forced and quasi-free vortex has moved to the vicinity of the outer wall, which is beneficial for droplets to move outward. Additionally, the droplets in HGRGS can be captured with enough residence time owing to the lower axial velocity than that in a typical cyclone.

Keywords: High gravity; Gas-liquid separator; Rotary drum; Pressure drop; Separation efficiency; Simulation.

NOMENCLATURE

a	inlet/outlet height
b	inlet/outlet width
B	droplets outlet diameter
C_D	drag coefficient
C_{ij}	convection term,
d_c	radial distance in a single channel
d_p	particle diameter
D	Separator diameter
D_e	drum diameter
$D_{l,ij}$	molecular diffusion term
$D_{t,ij}$	turbulent diffusion term
e	alternating symble
F_i	additional force
F_{ij}	rotation production term
g_i	acceleration of gravity
G_{ij}	buoyancy production term
h	cylindrical body height
H	Total height
i, j, k	1,2,3
L	length of rotary drum
p	pressure
p'	dispersion pressure
P_{ij}	shear production term
Re_p	Reynolds number of particle
R_{cx}	radius of the vortex core
S	drum height
S'	cross-sectional area
t	time
u	instantaneous velocity
u'	fluctuating velocity
$\bar{u}$	time average velocity
u_{pi}	particle velocity
v_x	axial velocity
$v_{\theta CS}$	tangential velocity
x	position
δ	kronecker factor
Δp	pressure drop difference
Δp_x	pressure loss in the vortex finder
Δp_{drum}	pressure loss in rotary drum
$\Delta p_{impeller}$	pressurization formed by the impeller
ε_{ij}	viscous dissipation term
η	viscosity coefficient of gas
μ	dynamic viscosity
ρ	gas density
ρ_p	particle density
φ_{ij}	pressure strain term

1. INTRODUCTION

The research results show that VOCs (volatile organic compounds) in industrial waste gases are directly related to the formation of PM 2.5 secondary aerosols and the VOCs from textile printing and dyeing industry have accounted for more than 30% (Han *et al.* 2018). Taking heat setting machine as an example, various dye and coating additives on textiles will be released in the form of gases during heat setting. Therefore, the textile industry is a serious disaster area of industrial waste gas (Hasanbeigi *et al.* 2015).

At present, the treatment of exhaust gas from printing and dyeing industry mainly focuses on the removal of oil fume. The common purification methods can be summarized into four categories: mechanical purification, spray washing, electrostatic precipitation and oxidation combustion. By means of mass force (Huang, 2011), filtration, adsorption and absorption (Yan *et al.* 2018), mechanical purification is more popular. Cyclone separators are the main centrifugal device to separate liquid from gas, but the efficiency in collecting particles less than 10 μm is low. Oleophilic polymer materials are used to remove the pollutants retained in the waste gas by filtration or adsorption. The initial effect is good, but the final effect will be worse and worse owing to the decreased surface area of polymer materials. Spray washing is an effective way to make the fume particles whose diameter is more than 2 μm fall off (Wu *et al.* 2017). However, the purified gas contains a lot of water or droplets. Electrostatic precipitation is a process to collect particles by charged plates (Jaworek *et al.* 2015). Since the exhaust gas with high temperature may cause the oily substances adhering to the electrode surface to fire, this method has more potential safety hazards. Combustion technology is widely used for low concentration organic waste gas and thus needs to add more supplementary fuels (Kamal *et al.* 2016). The biggest problem of combustion method is the tempering phenomenon. When there is a lot of grease stain, it may cause fires in the pipeline.

Through the introduction of the above-mentioned methods, we can clearly see that there are some defects in the individual treatment methods, as well as in meeting the emission requirements. To achieve the goal of cooling, oil fume purification and VOCs removal, we also try to adopt various combination processes to improve efficiency. Therefore, the project will combine spray washing and high gravity rotary gas-liquid separator (HGRGS) to deal with the exhaust gas with oil fume. Because the spray washing technology is relatively mature, the article will mainly focus on the research of HGRGS which is a newly designed device integrating cyclone separation technology and high gravity technology.

Cyclone has been demonstrated to have some advantages in gas-liquid separation and many researchers are trying to furtherly improve the separation performance. One is to exert an external force to the particles to change the force condition by applying an electric or magnetic field around the cyclone. Mazyan *et al.* (2016) studied the feasibility of the experiment by exerting magnetic force to improve the separation efficiency. Mazyan *et al.* (2017) also investigated electro-hydrodynamic forces which were applied by using particles containing electrostatic coatings. It indicated that the efficiency could be improved by 33% for 4 μm particle. In the investigation of Siadaty *et al.* (2017), a low intensity magnetic field was applied. For 2-4 μm particles, they found that the magnetic field increased the separation efficiency by 8.15% and 2.22%, respectively. The main advantage of this method was to increase separation efficiency without changing the pressure drop. A numerical simulation considering the effect of pulsing high voltage electrostatic field was carried out by Li *et al.* (2008). They drew the conclusion that the flow field velocity distribution curve inside the cyclone separator was similar to the velocity curve without the pulse electrostatic field, but the specific value had changed significantly. Besides, the electrostatic field had a stronger influence on the radial velocity of airflow.

On the other hand, rotary or dynamic components have been added to increase the centrifugal field. Through experiments and numerical simulations, Jiao *et al.* (2006, 2008) analyzed the flow field of the dynamic cyclone including rotary blades for different working conditions. Effects of backflow type dynamic cyclone were also presented (Chen *et al.* 2017), in which an impeller and a return pipe had been introduced internally. The designed separator had lower pressure drop and the efficiency exceeded 95% when the particles were larger than 5 μm. Besides, the rotational speed plays a critical role in the tangential velocity, rather than the treatment capacity. The similar conclusions were drawn by Zhou *et al.* (2014). Based on the conventional cyclone, another dynamic separator was experimented and simulated by them. They found that the geometric parameters including the number and inclination angle affected the separation performance by analyzing the structure of blades.

The cyclone performances are influenced by many geometric parameters. For example, choosing a reasonable diameter and vortex finder can further improve the separation efficiency and decrease the pressure drop (Brar *et al.* 2015; Ghodrat *et al.* 2013; Parvaz *et al.* 2017). In addition to the structural parameters of the vortex finder, the inlet structure parameters are also important (Cui *et al.* 2010). In the investigation of Misiulia *et al.* (2015, 2017), the cut size increased by increasing the inlet angle, but there was a reduction in collection efficiency. For the best performance, the inlet angle should be kept with 10-15°. In view of the inefficiency on 5-10 μm particles, the literature (Huang *et al.* 2018; Gao *et al.* 2018; Safikhani *et al.* 2016) had made some innovations and developed several new separators. These separators have reasonable pressure drop, and the separation efficiency is greatly improved.

HIGEE (High Gravity Rotary Device) is an effective method to intensify the relative velocity between phases under the supergravity condition (Zhao *et al.* 2010). The way to obtain supergravity is mainly to form a centrifugal force field by rotating the whole

or part of the equipment. HIGEE technology has become one of the most popular technologies in the chemical industry, and it has a promising prospect in many fields. Therefore, based on the HIGEE technology and cyclone, HGRGS is designed to separate the gas-liquid mixture after spray washing in the textile industry, in which a rotary drum with multi-layer fins and an impeller are applied.

Nowadays, numerical simulation has greatly promoted the research of experiment and theory. In this paper, the flow field of HGRGS is simulated by computational fluid dynamics. Subsequently, pressure drop, separation efficiency, distributions of the pressures and velocities are simulated and analyzed based on the RSM turbulence model.

2. SEPARATION PRINCIPLE AND NUMERICAL SIMULATION

2.1 Separation Principle

The schematic drawing of high gravity rotary gas-liquid separator (HGRGS) based on standard 2D2D cyclone (Safikhani *et al.* 2010) is shown in Fig. 1 and the main parameters are presented in Table 1. HGRGS is composed of inlet, droplets outlet, rotary drum, impeller and gas outlet, etc.

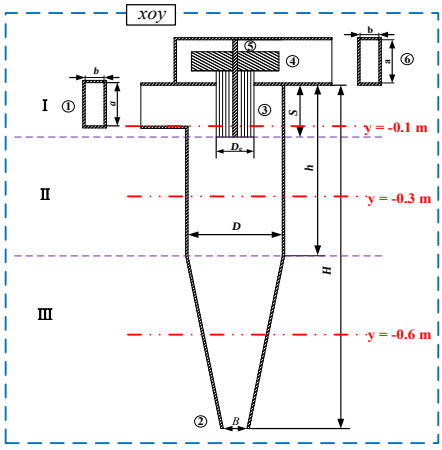

① inlet ② droplets outlet ③ rotary drum ④ impeller ⑤ rotary axis ⑥ gas outlet
I the separation region II the middle region III the bottom region

Fig. 1. Structure of HGRGS based on the standard 2D2D cyclone.

Table 1 The main structural parameters. (*D* = 0.2 m)

Parameter	Values
Separator diameter, *D/D*	1
Drum diameter, D_e/D	0.5
Inlet/outlet height, *a/D*	0.5
Inlet/outlet width, *b/D*	0.25
Drum height, *S/D*	0.625
Total height, *H/D*	4
Cylindrical body height, *h/D*	2
Droplets outlet diameter, *B/D*	0.25

Restricted by the cylinder wall, when the gas containing droplets axially enters the barrel, it will rotate downward and generate a centrifugal field to separate the suspended coarse droplets to the outer wall. Then, at the suction of the low-pressure zone acted by the upper impeller and shrinkage of the cone's diameter, a reversed upward spiral gas from the bottom is formed. Immediately the gas enters the rotary drum made up of multi-layer fins, it will rotate fast and thus the fine droplets will be separated again by the stronger centrifugal field. Subsequently, the clean gas flowing through the rotating impeller will be pressurized and finally discharged from the upper gas outlet. Owing to the existence of the rotary drum and impeller, HGRGS is characterized by low pressure drop and high efficiency.

2.2 Governing Equations

The incompressible Reynolds-averaged continuity and Navier-Stokes equations are solved and can be expressed as follows:

$$\frac{\partial u_i}{\partial x_i} = 0 \tag{1}$$

$$\frac{\partial}{\partial t}(\rho u_i) + \frac{\partial}{\partial x_i}(\rho u_i u_j) = -\frac{\partial p}{\partial x_i} + \left[\mu\left(\frac{\partial u_i}{\partial x_j} + \frac{\partial u_j}{\partial x_i} - \frac{2}{3}\delta_{ij}\frac{\partial u_i}{\partial x_i}\right) - \rho\overline{u_i' u_j'}\right] \tag{2}$$

In Eq. (2) , u_i is the velocity, x_i is the position, ρ is the constant gas density, p is the pressure, μ is the dynamic viscosity and the term $\overline{u_i' u_j'}$ is called Reynolds stress tensor, where $u_i' = u_i - \overline{u_i}$ is the fluctuating velocity component.

To close the equations and describe the turbulent behavior of flow, a new variable called Reynolds stress is introduced. Compared with other turbulence models in a cyclone, the Reynolds stress model (RSM) is more accurate to calculate the flow field (Cortes *et al.* 2007; Ma *et al.* 2000; Wang *et al.* 2007) and the transport equation is expressed as:

$$\underbrace{\frac{\partial\left(\rho\overline{u_i' u_j'}\right)}{\partial t}}_{C_{ij}} + \underbrace{\frac{\partial\left(\rho u_k \overline{u_i' u_j'}\right)}{\partial x_k}}_{C_{ij}} = \underbrace{-\frac{\partial\left(\rho\overline{u_i' u_j' u_k'} + \overline{p' u_i'}\delta_{kj} + \overline{p' u_j'}\delta_{ik}\right)}{\partial x_k}}_{D_{t,ij}} + \underbrace{\frac{\partial}{\partial x_k}\left[\mu\frac{\partial\left(\overline{u_i' u_j'}\right)}{\partial x_k}\right]}_{D_{l,ij}} - \underbrace{\rho\left(\overline{u_i' u_k'}\frac{\partial u_j}{\partial x_k} + \overline{u_j' u_k'}\frac{\partial u_i}{\partial x_k}\right)}_{P_{ij}} - \underbrace{\rho\beta\left(g_i\overline{u_j'\theta} + g_j\overline{u_i'\theta}\right)}_{G_{ij}} + \underbrace{\overline{P'\left(\frac{\partial u_i'}{\partial x_j} + \frac{\partial u_j'}{\partial x_i}\right)}}_{\phi_{ij}} - \underbrace{2\mu\overline{\frac{\partial u_i'}{\partial x_k}\frac{\partial u_i'}{\partial x_k}}}_{\varepsilon_{ij}} + \underbrace{2\rho\Omega_k\left(\overline{u_j' u_m'}e_{ikm} + \overline{u_i' u_m'}e_{jkm}\right)}_{F_{ij}} \tag{3}$$

where the first term is a transient term, C_{ij} is convection term, $D_{t,ij}$ is turbulent diffusion term, $D_{l,ij}$ is molecular diffusion term, P_{ij} is shear production term, G_{ij} is buoyancy production term , φ_{ij} is pressure

strain term, ε_{ij} is viscous dissipation term and F_{ij} is rotation production term.

To track the droplets when the volume fraction is less than 10%, the discrete phase model (DPM) is used and the one-way method is adopted, in which the flow field will affect the movement of droplets, while the influence of droplets on the continuum flow is very small. For a single particle, the equation of motion is given by:

$$\frac{du_{\mathrm{pi}}}{dt}=\frac{3\nu C_{\mathrm{D}}\,\mathrm{Re}_{\mathrm{p}}}{4\rho_{\mathrm{p}}d_{\mathrm{p}}^{2}}(u_i-u_{\mathrm{pi}})+\frac{(\rho_{\mathrm{p}}-\rho)g_i}{\rho_{\mathrm{p}}}+F_i \tag{4}$$

Here, for per unit particle mass, u_{pi} is the particle velocity, d_{p} is the particle diameter, ρ_{p} is the particle density, g_i is the acceleration of gravity, and F_i is the additional force, such as Magnus force and Basset force. The first term on the right side of Eq. (4) is the drag force and the drag coefficient, C_{D} can be expressed as:

$$C_{\mathrm{D}}=\frac{24}{Re_{\mathrm{p}}}(1+0.15Re_{\mathrm{p}}^{0.687}) \qquad Re_{\mathrm{p}}<1000 \tag{5}$$

$$C_{\mathrm{D}}=0.44 \qquad Re_{\mathrm{p}}\geq 1000 \tag{6}$$

Where Re_{p} is the Reynolds number of particle.

2.3 Simulation Strategy

The simulations are performed by the commercial software, ANSYS Fluent16.0. For the incompressible swirl inside the separator, the pressure-based solver coupled with RSM is adopted. In the simulation, the pressure interpolation format is PRESTO and the scheme conducted is the SIMPLEC scheme (Shukla *et al.* 2011). When calculating the momentum and turbulent kinetic energy, the second-order upwind scheme is selected, as well as the dissipation rate. Moreover, the sliding mesh method is used to simulate the rotating area including the drum and impeller. The three-dimensional model and mesh are shown Fig. 2 and the cross section of the rotary drum is presented in in Fig. 3.

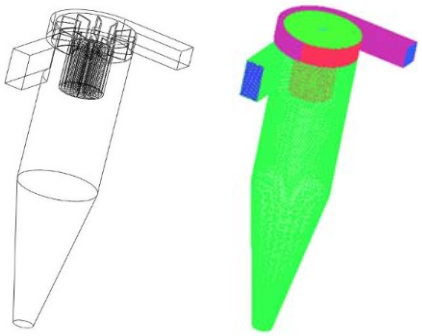

Fig. 2. The three-dimensional model and mesh.

2.4 Boundary Conditions

The continuous phase in the separator is air, and the inlet velocity is 10 m/s (normal to the inlet). The turbulence parameters are determined by turbulence intensity I = 0.042 and hydraulic diameter D_{H} = 0.067, where D_{H} is four times the radio of the inlet area and perimeter. Assuming that the flow at the exit is fully developed, gas and droplets outlets are both set as outflow. Besides, the impeller and drum with multi-layer fins are set as the rotating region and they are connected by interfaces for data transmission.

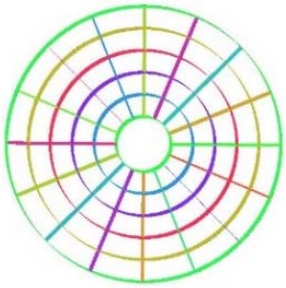

Fig. 3. The cross section of the rotary drum.

2.5 Mesh Independence Study

It is essential that the numerical results must be stable regardless of the grid number, which verifies the mesh independence to ensure the calculation accuracy. In this paper, the number of grids ranges from 3,962,959 to 6,521,553 for different separators. Table 2 shows the results of grid independency test. As is shown, the pressure drop between the inlet and gas outlet does not change significantly when the number of grids exceeds 5,677,605, hence the separator with 5,677,605 number of elements is appropriate.

Table 2 Results of grid independency test

Number of elements	Pressure drop (Pa)
3,962,959	328.56
4,969,551	161.05
5,677,605	105.63
5,831,009	97.83
6,521,553	100.09
7,938,776	103.21

2.6 Model Validation

To ensure the reliability of simulation, especially the RSM model, the computational data should be compared with the available results. The pressure drop is an important performance and the experimental, Wang model (Safikhani *et al.* 2010) and simulation results of a typical cyclone for different velocities are presented in Fig. 4. As is shown, the results have a good conformity for the velocity less than 16 m/s, but the error between CFD results and experiments increase gradually for larger velocity. The difference could be caused by the increase of turbulence at high velocity.

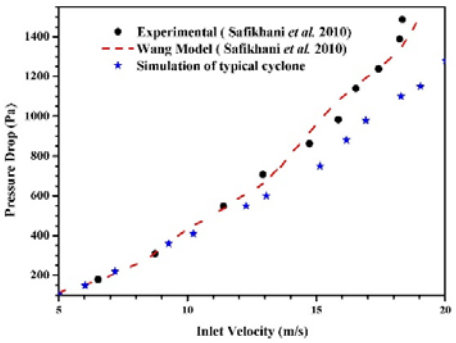

Fig. 4. Comparison between experimental, mathematical (Safikhani *et al.* 2010) and numerical results of typical cyclone.

3. RESULTS AND DISCUSSIONS

3.1 Pressure Drop and Flow Field Analysis

3.1.1 Pressure Drop

Figure 5 compares the pressure drop between HGRGS and typical cyclone (Safikhani *et al.* 2010). As is shown, the pressure drop in HGRGS is smaller than that in a cyclone. Owing to the forced vortex in the vortex finder, the flow is turbulent while that in the rotary drum is the laminar (Jiao *et al.* 2005). On the other hand, when the impeller inside the HGRGS rotates, the gas in the blade passage will move outward by the centrifugal force and thus producing the vacuum in the center. Driven by the pressure difference, the gas can be sucked up from the rotary drum, which makes up for the pressure loss in the separator and has the function of pressurization.

Owing to the cyclone's vortex finder is replaced by the rotary drum and an impeller in HGRGS, the pressure drop difference between them can be obtained by summing up the three parts as follows:

$$\Delta p = \Delta p_{\mathrm{x}} - \Delta p_{\mathrm{drum}} + \Delta p_{\mathrm{impeller}} \tag{7}$$

where Δp_{x}, Δp_{drum} is the pressure loss in the vortex finder and rotary drum, respectively, and $\Delta p_{\mathrm{impeller}}$ is the pressurization formed by the impeller.

Assuming axial velocity is uniform in the vortex finder, Δp_{x} can be expressed as (Hoffmann *et al.* 2002):

$$\Delta p_{\mathrm{x}} = \frac{\rho}{2} \times \frac{1}{\left(1 - R_{\mathrm{cx}}^2\right)^2} v_{\mathrm{x}}^2 + \frac{\rho}{2} \times \frac{1}{R_{\mathrm{cx}}^2} v_{\theta \mathrm{CS}}^2 \tag{8}$$

where v_{x} is the axial velocity, R_{cx} is the radius of the vortex core and $v_{\theta \mathrm{CS}}$ is the tangential velocity.

For the laminar flow in rotary drum, the pressure loss Δp_{drum} can be described according to the Hagen-Poiseuille formula :

$$\Delta p_{\mathrm{drum}} = \frac{8 \eta L S' v_{\mathrm{x}}}{\pi d_{\mathrm{c}}^4} \tag{9}$$

where η is the viscosity coefficient of gas, L is the length of rotary drum, S' is the whole cross-sectional area and d_{c} is the radial distance in a single channel.

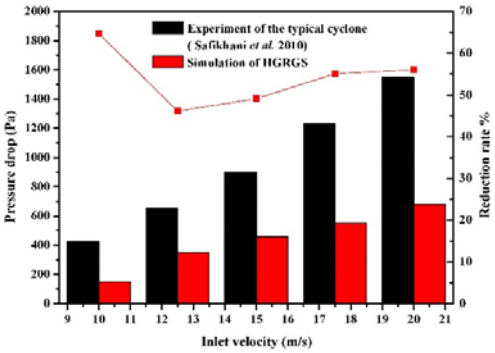

Fig. 5. Comparison of pressure drop between HGRGS and typical cyclone (Safikhani *et al.* 2010).

From Eqs. (7), (8) and (9), an expression can be derived for the pressure drop difference Δp:

$$\Delta p = \frac{\rho}{2} \times \frac{1}{\left(1 - R_{\mathrm{cx}}^2\right)^2} v_{\mathrm{x}}^2 + \frac{\rho}{2} \times \frac{1}{R_{\mathrm{cx}}^2} v_{\theta \mathrm{CS}}^2 - \frac{8 \eta L S v_{\mathrm{x}}}{\pi d_{\mathrm{c}}^4} + \Delta p_{\mathrm{impeller}} \tag{10}$$

From the above formulas, it is noted that the pressure loss is closely related to the axial velocity in the vortex finder or rotary drum. As the inlet velocity increases, the high axial velocity will contribute to the increase of Δp_{x} and Δp_{drum}. However, the pressure loss growth in the vortex finder is larger than the rotary drum. Because Δp_{x} is relative to the quadratic of the axial velocity, while Δp_{drum} is proportional to the axial velocity. Generally, the pressure drop difference increases gradually and it is clearly consistent with the trend in Fig. 5.

Compared with the typical cyclone, the maximum pressure drop reduction rate in HGRGS is 64.7% when the inlet velocity is 10 m/s, and the minimum reduction rate, which is 46.15%, occurs at 12 m/s. For larger velocity, there will be a slight improvement in reduction rate.

3.1.2 Static Pressure

The static pressure counters in the central section vertical to the inlet for HGRGS and typical cyclone are presented in Fig. 6. As is shown, the static pressure around the center is poor and it will increase as increasing the radius. When the downward gas reaches the bottom of the separator, it will turn to be the upward gas and then produce a tail wag structure, which makes the static pressure change to be the dynamic pressure. The static pressure has almost no change along the axial direction due to the less friction loss of the outer wall, and only a little change occurs in the inner area of the rotary drum. In Fig. 6b, the pressure gradient in a typical cyclone fluctuates at the inlet of the vortex finder and it indicates that the forced vortex (an important factor affecting the pressure drop) is generated. It should be noted that the centrifugal force generated by rotation is smaller than the radial pressure gradient and thus

the fine droplets will move to the central axis. As a result, it is difficult to deal with fine droplets escaping from the vortex finder with the upward gas. However, when the gas carrying fine droplets enters the drum with multi-layer fins in HGRGS, the low-speed gas will gradually be accelerated by the high-speed rotary drum. Accordingly, the static pressure in individual channel separated by fins will be changed into dynamic pressure, and fine droplets escaped from the first separation are captured to realize the secondary separation.

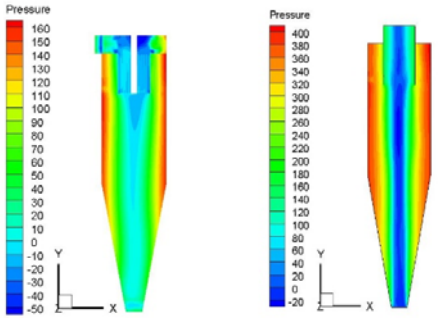

(a) (b)

Fig. 6. Static pressure counters in the central section vertical to the inlet for (a) HGRGS and (b) typical separator.

As is shown in Fig. 7, the trend of the static pressure distributions in HGRGS is similar to that in a typical cyclone, but there are some differences inside the rotary drum at the height of y = -0.1 m. The static pressure distribution of the vortex finder in the traditional cyclone is in the form of parabolic shape, while the static pressure distribution in the rotary drum of HGRGS is serrated. The drum is separated into five layers and the static pressure at each layer increases linearly with the increase of the radial distance. Because of the existence of the fin wall between two adjacent layers, the pressure is discontinuous and there can be more friction loss here.

3.1.3 Dynamic Pressure and Total Pressure

Dynamic pressure is closely associated to the axial velocity that it can indirectly reflect the magnitude of the velocity.

Dynamic pressure counters in the central section vertical to the inlet for HGRGS and typical cyclone are presented in Fig. 8. In the separation area I of the traditional cyclone, the dynamic pressure on the left side outside the vortex finder is obviously larger than that on the right side, which indicates that the gas has a great velocity when it enters the separator. Subsequently, caused by the expanded area of the flow region and inlet resistance, it will have a reduction in velocity on the right side. In the middle region II of a cyclone, the pressure at the center is the least and it will increase at first, then decrease along the radius direction. It is remarkable that the dynamic pressure around the interface between forced and quasi-free vortex is the maximum, because the velocity is the largest. Significantly, something has improved in HGRGS. The gas around the drum can be accelerated by the high-speed rotary drum and thus the dynamic pressure on the right side of the drum raises a lot compared with the typical cyclone. As is shown in Fig. 8a, the maximum dynamic pressure is between the drum and the outer wall, which makes the high-pressure area diffuse to the outer wall, then the occurrence of a secondary eddy can be reduced.

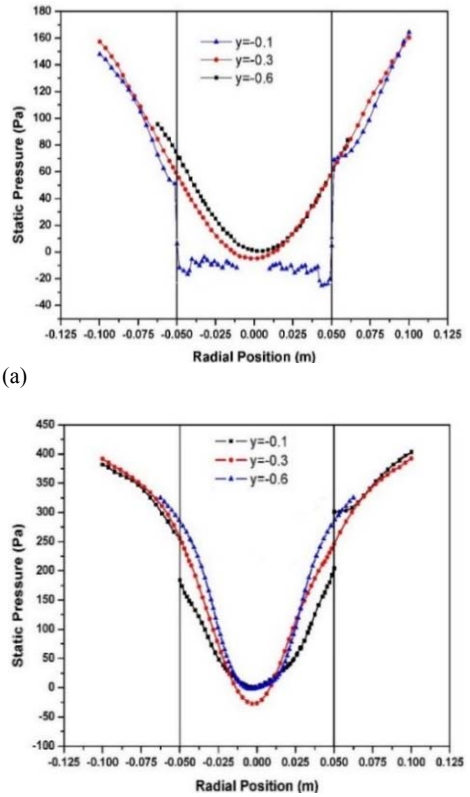

Fig. 7. Static pressure distributions along the radial direction at different heights in (a) HGRGS and (b) typical cyclone.

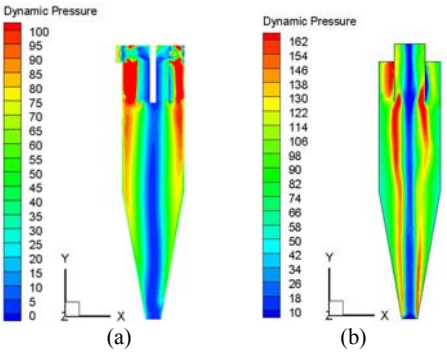

(a) (b)

Fig. 8. Dynamic pressure counters in the central section vertical to the inlet for (a) HGRGS and (b) typical cyclone.

Figure 9 compares the total pressure distribution counters of HGRGS and traditional cyclone. As is shown, the central pressure of the two separators is

the lowest and the pressure around the wall is the greatest, but the high-pressure area of the traditional cyclone is wider than that in HGRGS. Moreover, the pressure gradient inside the vortex finder changes a lot, while the pressure in the rotary drum is relatively uniform. At the outlet of the rotary drum in HGRGS, the flow direction changes from axial to radial when the gas enters the impeller passage, and then a central low-pressure region is formed. Consequently, driven by the pressure difference, the high-pressure gas under the rotary drum can flow to the upper low-pressure region, resulting in a lower pressure drop.

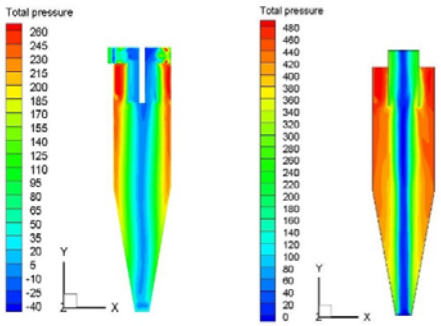

Fig. 9. Total pressure counters in the central section vertical to the inlet for (a) HGRGS and (b) typical separator.

In Fig. 10b, the total pressure inside the vortex finder is parabolic as the static pressure at the height of y = -0.1 m. The difference between the maximum and the minimum pressures can reach 300 Pa, while that in HGRGS is only 50 Pa. In Fig. 10a, the pressure in the drum increases in the direction of the radius, because the tangential velocity is proportional to the distance between the position and the center. The greater the distance is, the greater the tangential velocity and dynamic pressure, as well as the total pressure. Dominated by the rotary drum, the gas velocity in each layer eventually rotates with the rotary drum at the same speed, so the velocity and the pressure gradient in each layer have little change. Different from the static pressure curve, the total pressure of the traditional cyclone and HGRGS tends to decrease near the wall after the maximum pressure, which is beneficial to trap droplets by the pressure difference.

3.2 Separation Efficiency and Velocity Distribution

3.2.1 Collection Efficiency

In the view of Parvaz *et al.* (2017) and de Souza *et al.* (2012), despite the CFD model is sensitive to geometric changes, the discrete phase model and Lagrangian droplet trajectory analysis are also acceptable. Figure 11 compares the numerical efficiency in HGRGS and the experimental data in a cyclone. It shows that CFD results have the same trend with the experiment for droplets smaller than 14 μm. After that, the computational efficiency tends to be stable and it is almost 100%. It is worth mentioning that the separation performance in HGRGS is more efficient, especially for droplets smaller than 5 μm. Compared with the traditional separator, the efficiency of HGRGS at 1 μm can be greatly improved by 30%. This is mainly due to the rotary drum, which can form a stronger high gravity field to finish the secondary separation for fine droplets.

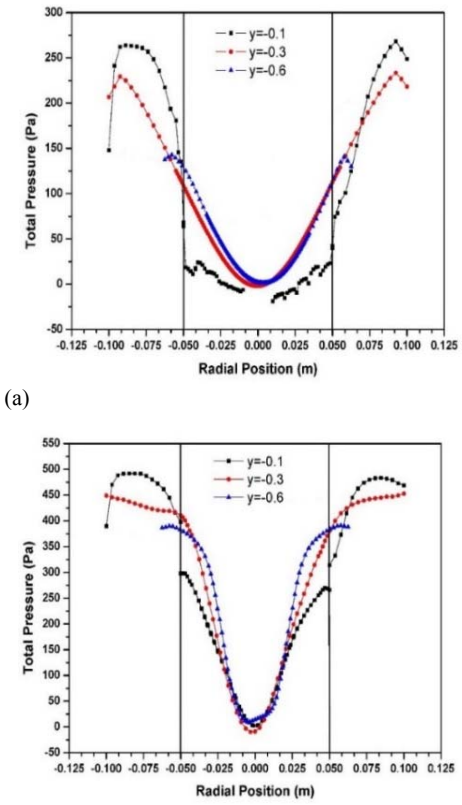

Fig. 10. Total pressure distributions along the radial direction at different heights in (a) HGRGS and (b) typical cyclone.

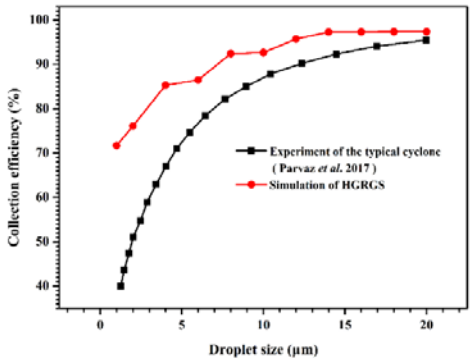

Fig. 11. Comparison of the numerical efficiency with experimental data (Parvaz *et al.* 2017).

3.2.2 Tangential Velocity

When the droplets in the flow field are affected by the high tangential velocity (the most important factor affecting the gas-liquid separation efficiency),

they will quickly slip, move outward, and then break away from the gas. Finally, the droplets are thrown to the outer wall by the density difference. At different heights in HGRGS, the tangential velocity distributions in the direction of the radius are shown in Fig. 12. As is shown, the tangential velocity has a good symmetry, and there is no great disturbance. HGRGS consists of three regions: the separation region with an area of the rotary drum, the middle region with barrel area and the bottom region with cone area. The velocity of these three regions increases first and then decreases along with the radial position from the middle axis to the wall. The separation area contains a rotary drum with high speed, which is the main part for the secondary separation. From the outside to the inside, the separation region can be divided into two parts: the annular region outside the rotary drum and the inner region with multi-layer fins. Inside the drum, the velocity at the height of y = -0.1 m is linear with the radius, corresponding to the formula for calculating the tangential velocity ($v_{tan} = \omega r$). Obviously, the higher the rotating speed, the greater the tangential velocity. In the outer annular space, the way of gas enters is tangential and when the gas rotates, the velocity will decrease with the increase of the flow-path, resulting in the difference of tangential velocity between the left and right sides of the rotary drum.

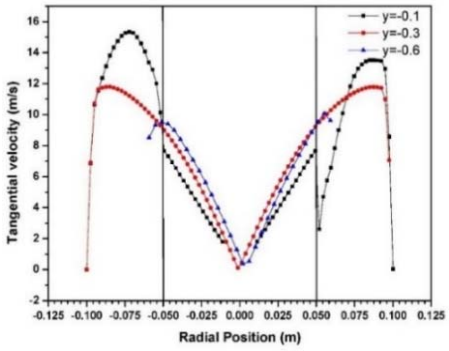

Fig. 12. Tangential velocity distributions along the radial direction at different heights in HGRGS.

At the height of y = -0.3 m in the middle region, the swirling flow of the typical cyclone can be divided into two parts. The inner part in the center is forced vortex that is similar to a rigid body, while the outer part is a quasi-free vortex. The transition position is approximately around the hypothetical extension surface under the vortex finder in Fig. 13b. Here, the maximum tangential velocity can generate the strongest centrifugal force, which can dominate the separation process and affect the separation efficiency. As is shown in Fig.13a, HGRGS has the same characteristics as a typical cyclone, but the transition position has expanded to the vicinity of the outer wall. As a result, it can further enlarge the area of the forced vortex. In the internal forced vortex region, the tangential velocity increases with the increase of radius, and thus it can produce a slow centrifugal force gradient, which is beneficial to the outward movement for droplets. When the tangential velocity reaches its maximum, it will decrease sharply and it is conducive to the separation of droplets by reducing kinetic energy.

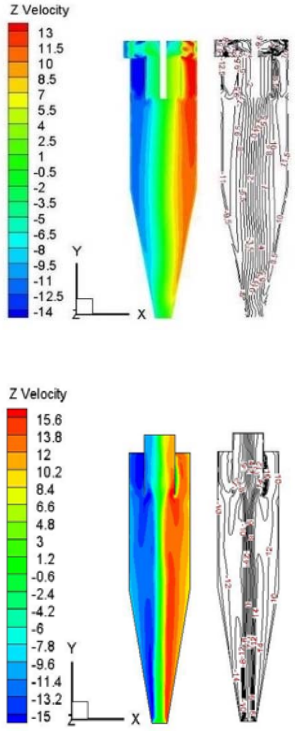

(a) (b)

Fig. 13. Tangential velocity counters and isolines in the central section vertical to the inlet for (a) HGRGS and (b) typical separator.

The bottom region of the separator refers to the area of the cone part, where mainly produces the internal vortex in the form of upstream flow. Caused by the shrinkage of the cross section, the velocity at the height of y = -0.6 m is close to the middle region.

3.2.3 Axial Velocity

To carry the droplets captured by the wall to the bottom, the axial velocity, especially the downward gas, plays an important role.

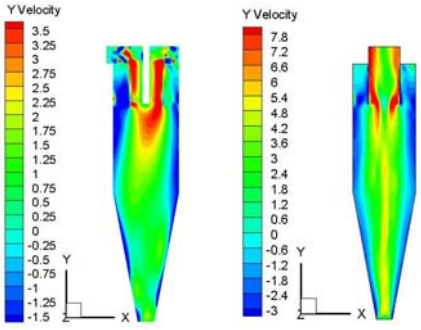

(a) (b)

Fig. 14. Axial velocity counters in the central section vertical to the inlet for (a) HGRGS and (b) typical separator.

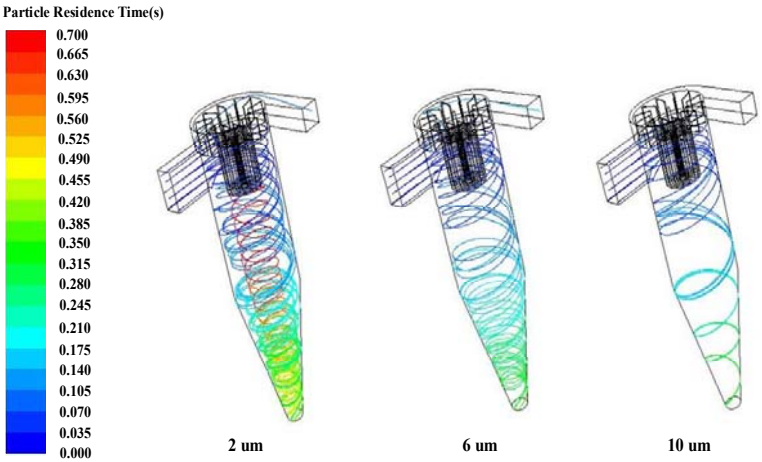

Fig. 15. Particle trajectories with diameter of 2 μm, 6 μm and 10 μm.

Axial velocity counters in the central section vertical to the inlet for HGRGS and typical separator are shown in Fig. 14. The axial velocity consists of two regions: upstream flow area and downstream flow area. As observed in Fig. 14, a zero axial velocity envelope plane is formed between the two flows. In the case of Fig. 14b, the envelope plane is obviously symmetrical. However, there is a 'swinging tail' in HGRGS. Owing to the existence of impeller, the movement of the gas is complicated and the upstream flow has more fluctuation.

In Fig. 14a, it is remarkably noted that the axial velocity in HGRGS is smaller than that in a typical cyclone and it is beneficial to the improvement of efficiency. It is assumed that the time for droplets to pass through the drum length is the same as the radial height. Then, $d_{p100\%}$, which is the smallest droplet can be collected with 100% probability, can be derived according to the equilibrium of forces. Based on the uniform axial velocity, $d_{p100\%}$ can be expressed as the following formula (Brouwers, 2002):

$$d_{p100\%} = \left(\frac{18\eta v_c d_c}{\rho_p \Omega^2 r L} \right)^{1/2} \tag{11}$$

where Ω is the angular velocity, r is the distance between the channel and the central axis. On the one hand, the low axial velocity can increase the droplet residence time and thus the droplets have enough time to reach the collecting wall. On the other hand, it can reduce the turbulence that a steady flow field can be provided for the movement of droplets.

3.3 Particle Trajectories

Figure 15 shows the particle trajectories with diameter of 2 μm, 6 μm and 10 μm. As is shown, the droplets with diameter of 2 μm have a good ability in following and more residence time. Controlled by the gas, droplets will rotate downward and then spiral up after reaching the cone part. Afterwards, fine droplets entering the rotary drum will conduct the second separation. However, due to the small size, some droplets that do not reach the bottom region may join in the internal updraft and finally escape from the gas outlet. Consequently, there is a low efficiency for 2 μm droplets.

Affected by larger centrifugal force, there are fewer rotating revolutions for 6 μm and 10 μm droplets. When droplets are thrown to the wall, they will slide down along the outer wall and be directly separated from the droplet outlet. It can also be seen that the inertia of 10 μm droplets is greater and it is easier to keep the original downward trajectory. Therefore, there is no escaping droplets discharged from the gas outlet, and the separation efficiency is higher.

4. CONCLUSIONS

The numerical simulation based on RSM method is performed to study the flow field of high gravity rotary gas-liquid separator (HGRGS). The results of pressure drop, separation efficiency, pressure distributions and velocity profiles at different heights are compared and analyzed. Combining the present results, the following conclusions can be drawn:

Compared with the typical cyclone, HGRGS has lower pressure drop and the maximum pressure drop reduction rate is 64.7% when the gas enters at 10 m/s. Moreover, the pressure drop difference between HGRGS and the typical cyclone increases gradually as increasing the inlet velocity.

Owing to the secondary separation conducted by the rotary drum, the separation efficiency in HGRGS is higher, especially for the droplets less than 5 μm. For 1 μm droplets, the efficiency of HGRGS can be greatly improved by 30%.

HGRGS has a symmetrical internal flow field. The tangential velocity inside the rotary drum is linear with the radius and it can be affected by the rotational speed. The higher the rotational speed, the greater tangential velocity and centrifugal force.

The area of the maximum tangential velocity where is the interface between the forced and quasi-free

vortex has moved to the vicinity of the outer wall in HGRGS, while that in the typical cyclone is around the hypothetical extension surface under the vortex finder. As a result, it can further enlarge the area of the forced vortex and produce a slow centrifugal force gradient in the internal forced vortex region, which is beneficial to the outward movement for droplets.

The axial velocity in the rotary drum is smaller than that in the typical cyclone. Consequently, the droplets can be captured with enough residence time.

Overall, the above-mentioned conclusions will contribute to the development of an efficient HGRGS. However, the current research is not enough, and other effects such as inlet velocity, structure of the rotary drum, distribution of droplets size and so on should be further studied. Finally, an optimized structure and operational strategies about HGRGS will be presented in the future.

ACKNOWLEDGEMENTS

This work was supported by the Introduce Talent Funding for Scientific Research at Nanjing Tech University (Grant No. 39802118) and Postgraduate Research & Practice Innovation Program of Jiangsu Province (KYCX19_0851).

REFERENCES

Brar, L. S., R. P. Sharma and R. Dwivedi (2015). Effect of Vortex Finder Diameter on Flow Field and Collection Efficiency of Cyclone Separators. *Particulate Science and Technology* 33(1), 34-40.

Brouwers, J. J. H. (2002). Phase separation in centrifugal fields with emphasis on the rotational particle separator. *Experimental Thermal and Fluid Science* 26(2), 325-334.

Chen, S., P. Liu and J. Gong (2017). Performance study of backflow type dynamic cyclone separator for coalbed methane. *Powder Technology* 305, 56-62.

Cortes, C. and A. Gil (2007). Modeling the gas and particle flow inside cyclone separators. *Progress in Energy and Combustion Science* 33(5), 409-452.

Cui, J., X. Chen and X. Gong (2010). Numerical Study of Gas−Solid Flow in a Radial-Inlet Structure Cyclone Separator. *Industrial & Engineering Chemistry Research* 49(11), 5450-5460.

de Souza, F. J., S. R. de Vasconcelos and M. D. A. de Moro (2012). Large Eddy Simulation of the gas–particle flow in cyclone separators. *Separation and Purification Technology* 94, 61-70.

Gao, S., D. Zhang and Y. Fan (2018). Separation Performance in a Novel Coupled Cyclone with Built-in Circulating Granular Bed Filter (C-CGBF). *Industrial & Engineering Chemistry Research* 57(36), 12192-12201.

Ghodrat, M., S. B. Kuang and A. B. Yu (2013). Computational Study of the Multiphase Flow and Performance of Hydrocyclones: Effects of Cyclone Size and Spigot Diameter. *Industrial & Engineering Chemistry Research* 52(45), 16019-16031.

Han, D., S. Gao, and Q. Fu (2018). Do volatile organic compounds (VOCs) emitted from petrochemical industries affect regional PM 2.5?. *Atmospheric Research* 209, 123-130.

Hasanbeigi, A. and L. Price (2015). A technical review of emerging technologies for energy and water efficiency and pollution reduction in the textile industry. *Journal of Cleaner Production* 95, 30-44.

Hoffmann, A. C. and L. E. Stein (2002). *Gas cyclones and swirl tubes: principles, design and operation.* Springer-Verlag Berlin Heidelgerg, Berlin, Germany.

Huang, L., S. Deng and Z. Chen (2018). Numerical analysis of a novel gas-liquid pre-separation cyclone. *Separation and Purification Technology* 194, 470-479.

Huang, X. (2011). CFD modeling of liquid–solid fluidization: Effect of drag correlation and added mass force. *Particuology* 9(4), 441-445.

Jaworek, A., A. Marchewicz and A. Krupa (2015). Dust particles precipitation in AC/DC electrostatic precipitator. *Journal of Physics: Conference Series* 646, 12031.

Jiao, J., Y. Zheng and G. Sun (2005). Numerical simulation of fine particle separation in a rotational tube separator. *China Particuology* 3(4), 219-223.

Jiao, J., Y. Zheng and G. Sun (2006). Study of the separation efficiency and the flow field of a dynamic cyclone. *Separation and Purification Technology* 49(2), 157-166.

Jiao, J., Y. Zheng and J. Wang (2008). Experimental and numerical investigations of a dynamic cyclone with a rotary impeller. *Chemical Engineering and Processing: Process Intensification* 47, 1861-1866.

Kamal, M. S., S. A. Razzak and M. M. Hossain (2016). Catalytic oxidation of volatile organic compounds (VOCs) – A review. *Atmospheric Environment* 140, 117-134.

Li, J. and W. Cai (2008). Numerical simulation of flow velocity distribution in cyclone with impulse electrostatic excitation. *Journal of Electrostatics* 66, 438-444.

Ma, L., D. B. Ingham and X. Wen (2000). Numerical modelling of the fluid and particle penetration through small sampling cyclones. *Journal of Aerosol Science* 31(9), 1097-1119.

Mazyan, W. I., A. Ahmadi and H. Ahmed (2017). Enhancement of solid particle separation

efficiency in gas cyclones using electro-hydrodynamic method. *Separation and Purification Technology* 182, 29-35.

Mazyan, W. I., A. Ahmadi and R. D. Jesus (2016). Use of ferrous powder for increasing the efficiency of solid particle filtration in natural gas cyclones. *Separation Science and Technology* 51(12), 2098-2104.

Misiulia, D., A. G. Andersson and M. T. S. Lundstr (2017). Effects of the inlet angle on the collection efficiency of a cyclone with helical-roof inlet. *Powder Technology* 305, 48-55.

Misiulia, D., A. G. Andersson and T. S. Lundström (2015). Effects of the inlet angle on the flow pattern and pressure drop of a cyclone with helical-roof inlet. *Chemical Engineering Research and Design* 102, 307-321.

Parvaz, F., S. H. Hosseini and G. Ahmadi (2017), *et al*. Impacts of the vortex finder eccentricity on the flow pattern and performance of a gas cyclone. *Separation and Purification Technology* 187, 1-13.

Safikhani, H. and P. Mehrabian (2016). Numerical study of flow field in new cyclone separators. *Advanced Powder Technology* 27(2), 379-387.

Safikhani, H., M. A. Akhavan-Behabadi and M. Shams (2010). Numerical simulation of flow field in three types of standard cyclone separators. *Advanced Powder Technology* 21(4), 435-442.

Shukla, S. K., P. Shukla and P. Ghosh (2011). Evaluation of numerical schemes using different simulation methods for the continuous phase modeling of cyclone separators. *Advanced Powder Technology* 22(2), 209-219.

Siadaty, M., S. Kheradmand and F. Ghadiri (2017). Improvement of the cyclone separation efficiency with a magnetic field. *Journal of Aerosol Science* 114, 219-232.

Wang, B., K. W. Chu and A. B. Yu (2007). Numerical Study of Particle−Fluid Flow in a Hydrocyclone. *Industrial & Engineering Chemistry Research* 46(13), 4695-4705.

Wu, X., Y. Yu and Z. Qin (2017). Performance of CO_2 absorption in a diameter-varying spray tower. *Chinese Journal of Chemical Engineering* 25(8), 1109-1114.

Yan, S., W. Huo and J. Yang (2018). Green synthesis and influence of calcined temperature on the formation of novel porous diatomite microspheres for efficient adsorption of dyes. *Powder Technology*. 329, 260-269.

Zhao, H., L. Shao and J. Chen (2010). High-gravity process intensification technology and application. *Chemical Engineering Journal* 156(3), 588-593.

Zhou, Y., Z. Mingfei and C. Ma (2014). Experimental and numerical investigations of a dynamic cyclone. *Proceedings of the Institution of Mechanical Engineers, Part A: Journal of Power and Energy* 228(5), 536-549.